Efficient and dynamic nuclear localization of green fluorescent protein *via* RNA binding

CrossMark

Akira Kitamura, Yusaku Nakayama, Masataka Kinjo[*]

Laboratory of Molecular Cell Dynamics, Faculty of Advanced Life Science, Hokkaido University, Sapporo, Japan

ABSTRACT

Classical nuclear localization signal (NLS) sequences have been used for artificial localization of green fluorescent protein (GFP) in the nucleus as a positioning marker or for measurement of the nuclear-cytoplasmic shuttling rate in living cells. However, the detailed mechanism of nuclear retention of GFP-NLS remains unclear. Here, we show that a candidate mechanism for the strong nuclear retention of GFP-NLS is *via* the RNA-binding ability of the NLS sequence. GFP tagged with a classical NLS derived from Simian virus 40 (GFP-NLS^{SV40}) localized not only in the nucleoplasm, but also to the nucleolus, the nuclear subdomain in which ribosome biogenesis takes place. GFP-NLS^{SV40} in the nucleolus was mobile, and intriguingly, the diffusion coefficient, which indicates the speed of diffusing molecules, was 1.5-fold slower than in the nucleoplasm. Fluorescence correlation spectroscopy (FCS) analysis showed that GFP-NLS^{SV40} formed oligomers *via* RNA binding, the estimated molecular weight of which was larger than the limit for passive nuclear export into the cytoplasm. These findings suggest that the nuclear localization of GFP-NLS^{SV40} likely results from oligomerization mediated *via* RNA binding. The analytical technique used here can be applied for elucidating the details of other nuclear localization mechanisms, including those of several types of nuclear proteins. In addition, GFP-NLS^{SV40} can be used as an excellent marker for studying both the nucleoplasm and nucleolus in living cells.

© 2015 Elsevier Inc. All rights reserved.

1. Introduction

The nucleus is an important organelle in eukaryotic cells in which physiological functions including storage and read-out of genetic information are carried out. In the nucleus, the nucleolus, which is the largest structure, plays an important role as the location of ribosome biogenesis [1]. To form a complex between ribosomal RNA and ribonucleoproteins, members of a family of small nucleolar RNAs (snoRNAs) function as targets for RNA-modification enzymes [1]. Recently, the relationship between homeostasis in the nucleolus and the onset of many diseases, including cancer and neuronal disease, has been discussed [2,3]. The region outside of the nucleolus is called the nucleoplasm, which contains substances such as nucleotides and proteins. The nucleus is surrounded by a double lipid bilayer membrane. In order for components to shuttle between the nucleus and the cytoplasm, the nuclear membranes are permeated by channels called nuclear pore complexes (NPCs) [4]. The diameter of the NPC channel is approximately 5–10 nm [4,5]. Biomolecules smaller than the diameter of the NPC channel can diffusively pass through the channel, while larger molecules (>50 kDa) and complexes cannot pass through [5]. To efficiently transport substrate proteins into the nucleus, recognition of a nuclear localization signal (NLS) peptide in the cargo protein by nucleo-cytoplasmic transporters, such as importin family proteins and RanGTP, is crucial [5].

Two classes of NLS are known. One class comprises classical NLSs enriched with lysine amino acids [6], and the other is made up of non-classical NLSs [5]. The first classical NLS was identified in the Simian virus 40 (SV40) large T antigen [7], which is first recognized by importin α, a nuclear transport receptor containing a bipartite NLS, and then recognized by importin β for transport into the nucleus [6]. The best defined classical NLSs are those of the SV40 large T antigen and nucleoplasmin [5,6]. On the other hand, many types of proteins with non-classical NLSs have been identified, such as the acidic M9 domain of heterogenous ribonucleo-protein (hnRNP) A1 and the complex signals of U snRNPs, spliceosomal ribonucleo-proteins [5]. These proteins are directly recognized by importin β

without the intervention of an importin α-like protein [5]. Moreover, proline−tyrosine NLSs (PY-NLS) have been recently identified [8]. PY-NLS sequences are recognized by importin β2, which transports the PY-NLS-containing protein into the nucleus [8].

NLSs have been used for artificial localization of proteins of interest (e.g., fluorescent/luminescent protein) [9–11]. In particular, many types of fluorescent proteins (FP) tagged with an NLS (FP-NLS) have been engineered as nuclear markers, as well as FP tagged with functional nuclear proteins (e.g., histone H2B, ERK1, and importin β) [9,12]. However, the mechanism that mediates the nuclear localization of artificial model proteins remains unclear, and FP-NLSs exhibit variable localization in the nucleus and are sometimes mislocalized to the cytoplasm. Here, we show that NLS-tagged monomeric GFP is efficiently localized in the nucleus, and that this localization is mediated *via* binding to RNA in the nucleolus.

2. Materials and Methods

2.1. Plasmid construction

The EGFP fragment in a pEGFP-C1 plasmid vector (Clontech, Mountain View, CA) was substituted to meGFP carrying A206K, a monomeric variant of eGFP, to generate pmeGFP-C1 [13]. To create meGFP tagged with an NLS, synthetic oligo-DNAs encoding three tandem repeats of NLS derived from SV40 (PKKKRKVPKKKRKVPKKKRKV) [7] or poly (ADP-ribose) polymerase (PARP; VKSEGKRKGGEVAKKKSKKEKDKDSKLEKALKAE) [14] (Life Technologies, Waltham, MA) were annealed and inserted into pmeGFP-C1 *via* the BglII and HindIII restriction sites (GFP-NLS). The sequences were confirmed using a genetic analyzer (Applied Biosystems, Waltham, MA) and correct clones were selected. To generate a nucleolus marker, mCherry-fibrillarin, cDNA coding for fibrillarin was inserted into a pmCherry-C1 vector [15].

2.2. Cell culture and transfection

Mouse neuroblastoma Neuro2A cells were maintained in Dulbecco's Modified Eagle's Medium (DMEM; Sigma-Aldrich, St. Louis, MO) supplemented with 10% FBS (GE Healthcare, Logan, UT), 100 units/ml penicillin G (Sigma-Aldrich), and 100 μg/ml streptomycin (Sigma-Aldrich) at 37 °C and 5% CO_2. A plasmid mixture comprising 100 ng GFP- or GFP-NLS-carrying vector and 900 ng pCAGGS was transfected into Neuro2A cells using 2.5 μl of Lipofectamine 2000 (Life Technologies). For live-cell analysis, cells were cultured on glass-based 3.5 cm dishes (3910-035; Asahi-Technoglass, Tokyo, Japan).

2.3. Confocal fluorescence microscopy

Neuro2A cells expressing GFP-NLSs and mCherry-fibrillarin were stained with 1.0 μg/ml Hoechst 33342 (Sigma-Aldrich) for 30 min at 37 °C and 5% CO_2 atmosphere. After washing three times in Hank's balanced salt solution (HBSS; Sigma-Aldrich), fresh medium was added to the plate and the cells were observed on an LSM 510 META confocal microscope (Carl Zeiss, Jena, Germany) through a C-Apochromat 40 × /1.2NA W Korr UV-VIS-IR M27 water immersion objective on a heat stage incubator at 37 °C in a 5% CO_2 atmosphere. Hoechst33342, GFP, and mCherry were sequentially excited at 405 nm, 488 nm, and 594 nm, respectively. Excitation beams were split by an HFT405/488 filter for Hoechst33342 and GFP, or an HFT405/514/594 filter for mCherry. Hoechst 33342 and GFP fluorescence were separated by a dichroic mirror (NFT490) and collected through BP420-480 and BP505-550 band pass filters, respectively. Fluorescence from mCherry was collected through a NFT595 filter and a spectro-photodetector (META) at 615−754 nm. The pinhole size for Hoechst33342, GFP, and mCherry was set at 1.0 airy unit: 61 μm, 72 μm, and 94 μm, respectively. Zoom factor was set at 5-fold. X- and Y-scanning sizes were each 512 pixels. The microscope operated on an AIM 4.2 software platform (Carl Zeiss). Acquired images were adjusted using ImageJ 1.47v (National Institutes of Health, Bethesda, MD) and Photoshop CS4 (Adobe Systems, San Jose, CA).

2.4. Fluorescence recovery after photobleaching (FRAP)

Photobleaching experiments were performed on an LSM 510 META using a C-Apochromat 40×/1.2NA W Korr UV−VIS−IR water immersion objective (Carl Zeiss). GFP was excited (41.1 μW) and photobleached (723 μW) at 488 nm. X- and Y-scanning sizes were 256 and 100 pixels, respectively. Image acquisition scanning time was set at 97 ms/frame. The photobleaching period was 232 ms. Relative fluorescence intensity was measured using AIM3.2 software platform (Carl Zeiss) and calculated according to Axelrod's method [16]. The recovery curve of relative fluorescence intensity was fitted with the equation derived by Soumpasis [17] on Origin 2015 software (OriginLab Corp., Northampton, MA), and diffusion time (τ_D) and maximum recovery rate were obtained. The radius of the photobleached area ($w = 1.22 \pm 0.137$ μm; n = 6) was obtained from images of 4% paraformaldehyde-fixed cells expressing GFP-NLS[SV40] according to Axelrod's method [16]. The diffusion coefficient (D) was calculated according to the relationship between diffusion time and the radius of the photobleached area: $D = w^2/4\tau_D$.

2.5. Fluorescence correlation spectroscopy (FCS)

FCS measurements were performed using a ConfoCor 3 system combined with an LSM 510 META microscope (Carl Zeiss) using a C-Apochromat 40 × /1.2NA W Korr UV-VIS-IR M27 water immersion objective (Carl Zeiss). The confocal pinhole diameter was adjusted to 70 μm. GFP was excited at 488 nm and emission signals were detected using a 505 nm long-pass filter. To prepare cell lysate containing GFP or GFP-NLS, cells expressing GFP or GFP-NLS were washed in PBS and then solubilized in lysis buffer containing 50 mM Hepes-KOH (pH 7.5), 150 mM NaCl, 1% Triton X-100, and 1% Protease inhibitor cocktail (Sigma-Aldrich) at 4 °C. After centrifugation at 15,000 rpm for 15 min at 4 °C, supernatants were recovered. Dialyzed recombinant ribonuclease I_f (RNase I_f; New England BioLabs, Ipswich, MA) in 10 mM Tris-HCl (pH 8.0) or the same volume of Tris-HCl buffer as a negative control was added to the cell lysate at a 1/10 dilution (250 units total) and incubated for 30 min at 25 °C. The cell lysates were then measured and analyzed using AIM 4.2 and ZEN 2012 software (Carl Zeiss), as described previously [18–20]. The optical system and structure parameters were calibrated by measurement of rhodamine 6G. The diffusion coefficient was calculated using that of rhodamine 6G as a standard (414 μm²/s). Molecular weights were calculated from the ratio of the diffusion coefficient to GFP monomer (27 kDa) according to the Stokes−Einstein relation [18].

Statistical significance was determined by Student's *t*-test.

3. Results

3.1. Nuclear and nucleolar localization of GFP-NLS[SV40]

To observe the nuclear localization of NLS-tagged GFP in living Neuro2A cells, confocal fluorescence microscopy was performed. We prepared expression plasmids coding for monomeric GFP tagged with three tandem repeats of a classical NLS derived from SV40

(GFP-NLS^{SV40}) or a single repeat of the NLS sequence modified from PARP (GFP-NLS^{PARP}). Fluorescent signals from non-tagged control GFP were distributed throughout the cytoplasm (Fig. 1A–D). Conversely, GFP-NLS^{SV40} was localized in the nucleus, and no fluorescent signals were observed in the cytoplasm. GFP-NLS^{SV40} produced a speckled pattern of high intensity GFP that colocalized with mCherry-fibrillarin, which was used as a nucleolus marker protein (Fig. 1E–H), indicating that GFP-NLS^{SV40} accumulated not only in the nucleoplasm, but also in the nucleolus. Next, we assessed the localization of GFP-NLS^{PARP}. GFP-NLS^{PARP} was also localized to the nucleus, but some fluorescent signal was also observed in the cytoplasm (Fig. 1I–L). The intensity of GFP-NLS^{PARP} in the nucleolus was lower than that of GFP-NLS^{SV40} but higher than that of control GFP (Fig. 1A, E, and I). These results suggest that strong retention in the nucleolus may be required for precise nuclear localization, and that GFP-NLS^{SV40} is suitable as a nucleus marker.

3.2. Dynamic accumulation of GFP-NLS^{SV40} in the nucleolus

We next examined whether GFP-NLS^{SV40} forms immobile inclusion bodies in the nucleus. To determine this, the mobility of the protein in living cells was analyzed by fluorescence recovery after photobleaching (FRAP), which can measure the mobile or immobile properties of a fluorescent molecule based on the recovery rate of fluorescence intensity after a brief period of photobleaching [12,16,17]. The fluorescence intensity of GFP-NLS^{SV40} in the nucleolus and nucleoplasm recovered immediately after photobleaching (Fig. 2, A and B). The maximum recovery rate in the nucleolus was 105% ± 2.82% (mean ± S.D.; n = 10), and this was similar in the nucleoplasm (102% ± 3.44%; n = 11). This indicates that GFP-NLS^{SV40} is mobile in both the nucleoplasm and nucleolus, and that accumulation in the nucleolus is not the result of formation of inclusion bodies. To quantitatively compare the mobility of GFP-NLS^{SV40} between the nucleolus and nucleoplasm, the diffusion coefficient (D), a physical value that can be compared to previously obtained values in same environment (e.g., living cells), was calculated from the recovery curve. The D value in the nucleolus (3.48 ± 1.06 μm^2/s; n = 10) was significantly smaller than in the nucleoplasm (5.92 ± 2.95 μm^2/s; n = 11, $p < 0.05$), suggesting that GFP-NLS^{SV40} interacts with some component in the nucleolus.

3.3. Oligomerization of GFP-NLS^{SV40} via RNA

Numerous proteins and RNAs are functionally accumulated in the nucleolus. Thus, we hypothesized that RNA may play a key role in the nucleolar localization of GFP-NLS^{SV40}. To examine the contribution of RNA to the nucleolar localization of GFP-NLS^{SV40}, we first determined whether the molecular size of GFP-NLS^{SV40} was changed by RNase treatment. This was examined using fluorescence correlation spectroscopy (FCS), in which the diffusion coefficient and brightness of single fluorescence molecules in solution with single molecule sensitivity can be obtained by analysis of fluorescence fluctuation [18,20–22]. First, we evaluated the shape
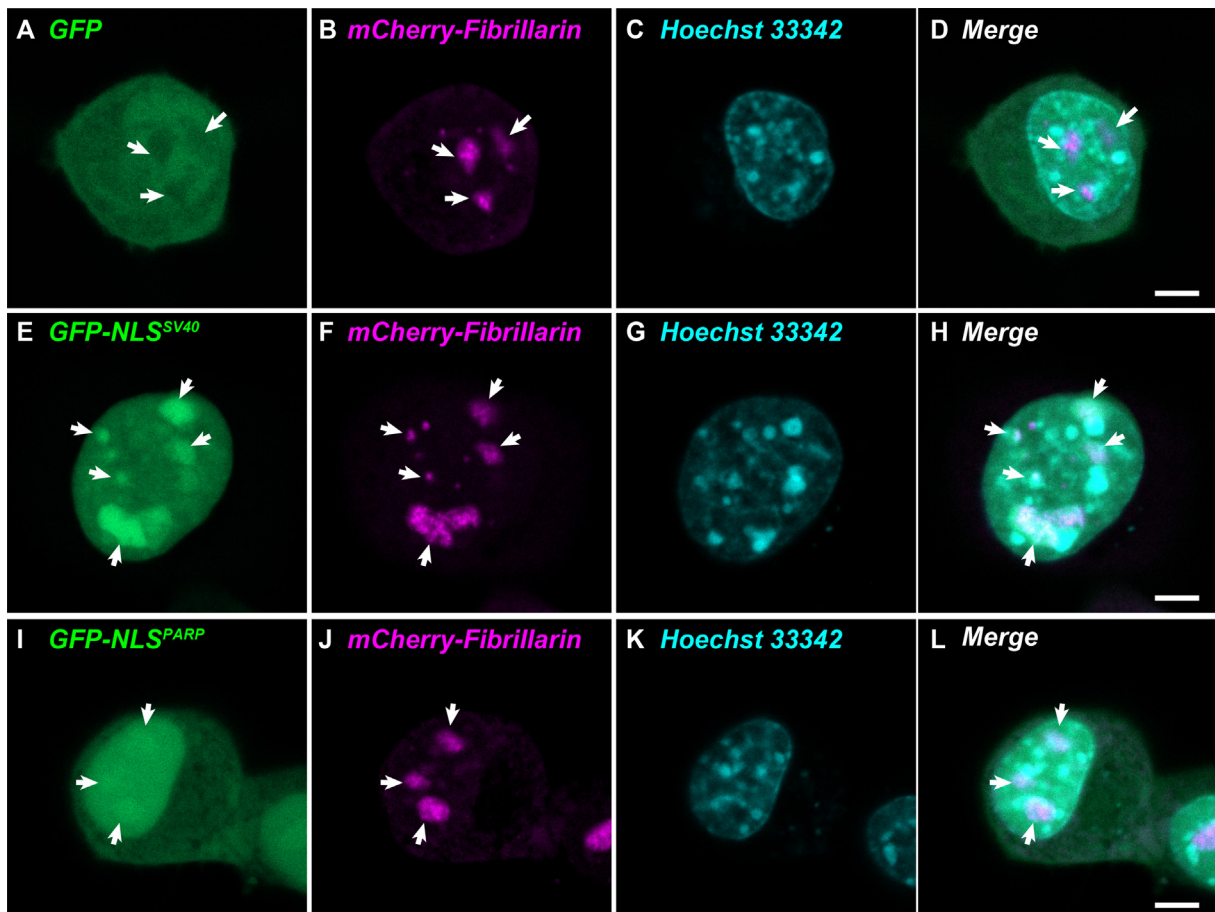

Fig. 1. Intracellular localization of GFP-NLS^{SV40} and GFP-NLS^{PARP} revealed by fluorescence confocal laser scanning microscopy. White arrows indicate the position of the nucleolus. Scale bar = 5 μm.
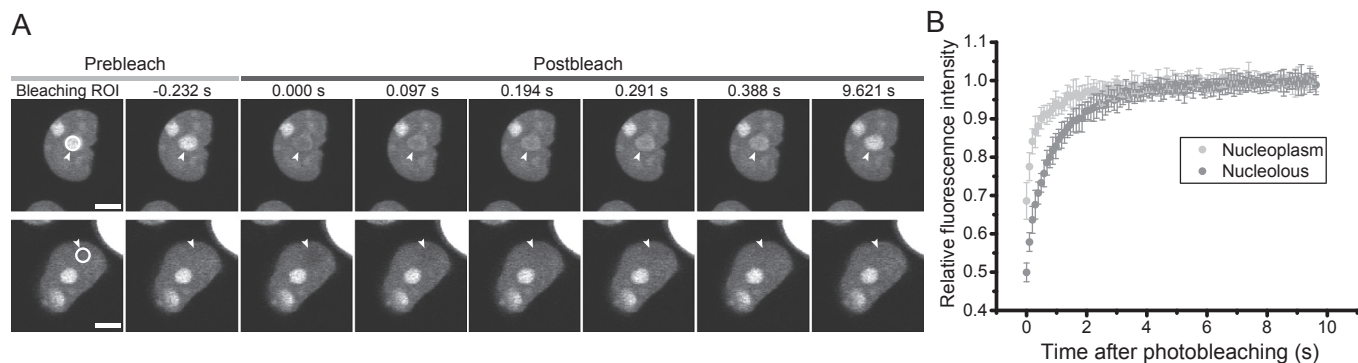
Fig. 2. FRAP analysis of the mobility of GFP-NLS[SV40] in the nucleolus in living cells. (A) A typical image series of GFP-NLS[SV40] during FRAP experiments. The white circle in the prebleach image indicates the target area for photobleaching. Scale bar = 5 μm. (B) Time-course of recovery of relative fluorescence intensity. Dots and error bars indicate the mean value and S.D., respectively (n = 11 for nucleoplasm and n = 10 for nucleolus).

of the auto-correlation functions (ACFs), which indicate the residence time of fluorescence molecules in the detection volume. The ACF of GFP-NLS[SV40] in cell lysate showed a right-shift compared with that of control GFP (Fig. 3A), indicating that GFP-NLS[SV40] forms a large molecular weight complex. In agreement with this, the ACF of GFP-NLS[SV40] treated with RNase was shifted to left compared to non-treated GFP-NLS[SV40] (Fig. 3B), but no change was observed in the ACF of GFP before and after treatment with RNase (Fig. 3C). These results suggest that GFP-NLS[SV40] forms a complex with RNA.

Next, to quantitatively determine the assembly state of the molecules, we performed one- and two-component model curve fitting analysis for GFP and GFP-NLS[SV40], respectively. This was necessary because the one-component model was sufficient to determine the ACF of GFP but not of GFP-NLS[SV40]. All values obtained by the fitting analysis are shown in Fig. 4. Counts per molecule (CPM), which indicates the mean molecular brightness of the fluorescent particle, showed a 3-fold increase in GFP-NLS[SV40] compared with GFP (Fig. 4A, lanes 1 and 3). RNase treatment decreased the CPM of GFP-NLS[SV40] (Fig. 4A, lanes 3 and 4) but did not change the CPM for GFP (Fig. 4A, lanes 1 and 2). These results indicate that GFP-NLS[SV40] forms oligomers *via* binding to RNA and suggest that the oligomers contain at least three GFP molecules. The component of the sample exhibiting a large diffusion coefficient was defined as the fast component. Although the diffusion coefficient of the fast component (D_{Fast}) of GFP was not changed by RNase treatment (Fig. 4B, lanes 1 and 2), the D_{Fast} of GFP-NLS[SV40] was significantly increased by RNase treatment (Fig. 4B, lanes 3 and 4) and was significantly lower than that of GFP (Fig. 4B, lanes 1, 2, and 4). Although no significant change in the D_{Slow} of GFP-NLS[SV40] was observed (Fig. 4C), the portion of GFP-NLS[SV40] defined as the

fast fraction was significantly increased by RNase treatment (Fig. 4D). These results suggest that degradation of RNA causes disassembly of GFP-NLS[SV40] oligomers.

Next, we estimated the molecular weight (M_w) of GFP-NLS[SV40] using the D_{Fast} value and the Stokes−Einstein relation (see Materials and Methods). The M_w of GFP-NLS[SV40] without RNase treatment was ~1.6 MDa. However, although the normalized CPM value suggests that GFP-NLS[SV40] exists as a trimer, the calculated M_w of GFP-NLS[SV40] was significantly larger than that of a GFP trimer (the M_w of monomeric GFP was 27 kDa). The M_w of GFP-NLS[SV40] after treatment with RNase was 121 kDa; this value was larger than the M_w of GFP-NLS[SV40] monomer evaluated from amino acids composition, which was 32 kDa. These results suggest that the oligomers that form between GFP-NLS[SV40] and RNA also contain endogenous proteins, thereby forming a large complex that is retained in the nucleus.

4. Discussion

In this study, we showed that GFP tagged with three tandem repeats of NLS derived from SV40 (GFP-NLS[SV40]) was clearly localized in the nucleus and not in the cytoplasm. However, GFP-NLS[PARP] was partially mislocalized in the cytoplasm (Fig. 1), indicating that between the two, GFP-NLS[SV40] is more suitable as a nuclear marker. What is the mechanism that drives this clear nuclear localization? Molecules with a molecular weight less than approximately 50 kDa are able to pass passively through the NPC [5]. Therefore, GFP monomers diffusely move between the nucleus and the cytoplasm [22]. The estimated molecular weight of GFP-NLS[SV40] determined from the diffusion coefficient after treatment with RNase was 121 kDa (calculated from the results in Fig. 4). This
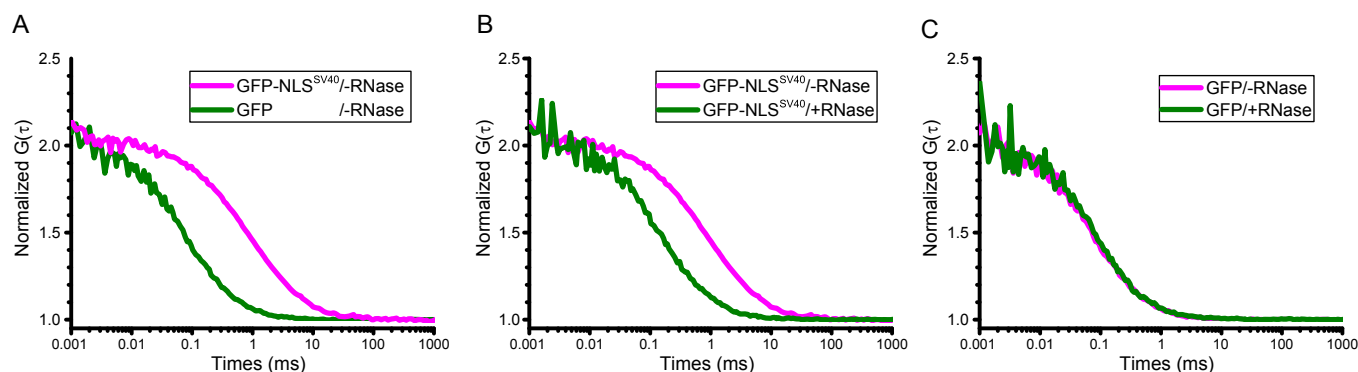

Fig. 3. Normalized auto-correlation functions (ACFs) of cell lysates of Neuro2A cells expressing GFP or GFP-NLS[SV40]. (A) Comparison between GFP and GFP-NLS[SV40] without RNase treatment. (B) Comparison of GFP-NLS[SV40] with and without RNase treatment. (C) Comparison of GFP with and without RNase treatment.
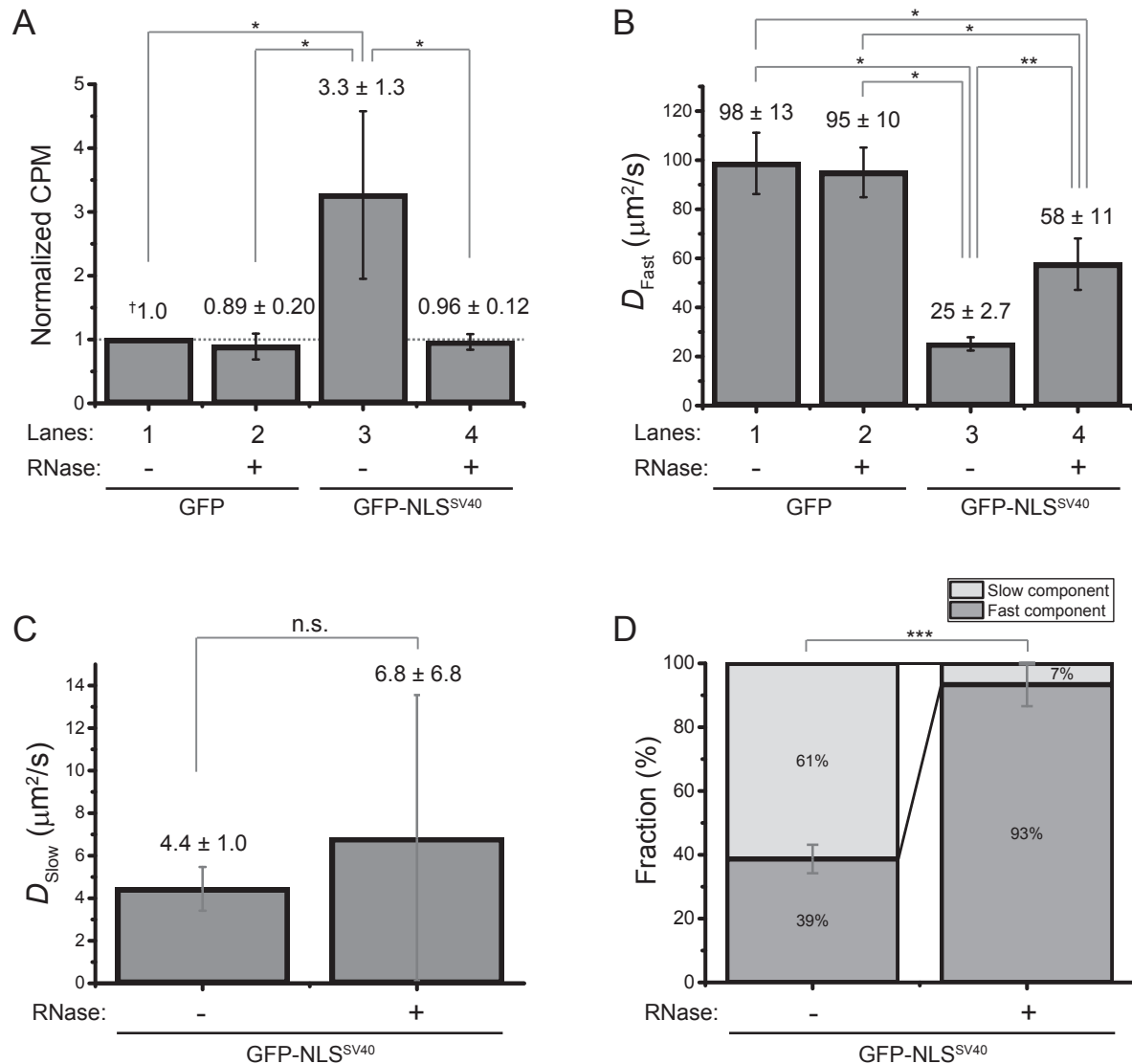
Fig. 4. Curve fitting analysis of FCS measurements. Numerical values in the graph indicate the mean value ± S.D. (n = 3). Student's *t*-test: $^*p < 0.05$, $^{**}p < 0.005$, $^{***}p < 0.001$. (A) Normalized CPM values of GFP with and without RNase treatment are shown. The gray dashed line indicates a CPM value of 1.0. † denotes the normalization value. (B) The diffusion coefficient of the fast component. For GFP, diffusion coefficients obtained by one-component curve fitting analysis are shown. (C) Diffusion coefficients of the slow component of GFP-NLS[SV40]. (D) Comparison of the fraction of fast and slow components of GFP-NLS[SV40] with and without RNase treatment.

suggests the formation of a complex with endogenous proteins that is larger than the molecular weight limit for passive diffusion through the NPC. If GFP-NLS[SV40] transported into the nucleus after translation forms a complex of at least 121 kDa with other proteins, it cannot be exported into the cytoplasm without the assistance of a nuclear export mechanism. A likely explanation for the clear localization of GFP-NLS[SV40] in the nucleus is that the complex of oligomeric species formed between RNA and GFP-NLS[SV40] retard nuclear export. On the other hand, fluorescence correlation spectroscopy was used to evaluate the assembled states of GFP-NLS[SV40] (Figs. 3 and 4). The estimated molecular weight of GFP-NLS[SV40] determined from the fast diffusion coefficient without RNase treatment was approximately 1.6 MDa. This is similar to the molecular weight of the 40S ribosome (1.4 MDa) [23], suggesting that GFP-NLS[SV40] may interact with ribosomal RNA. In addition, the molecular weight estimated from the slow diffusion coefficient without RNase treatment was ~300 MDa, suggesting that GFP-NLS[SV40] interacts with multiple partners. However, the diffusion coefficients of GFP-NLS[SV40] measured in the nucleoplasm and

nucleolus in living cells were very fast with no evidence of an immobile fraction (Fig. 2). This agrees with the previously reported slow component of monomeric GFP in living cells [22], suggesting that the association and dissociation rate between GFP-NLS[SV40] and its interacting partners in living cells may be quite rapid. One possible explanation for the fast diffusion rate in living cells is that hydrolysis of nucleotides (e.g., ATP and/or GTP) may contribute to the transient dissociation of the large molecular weight complex. What are the interacting partners of GFP-NLS[SV40]? Unfortunately, FCS cannot directly identify interacting partners of proteins and/or RNAs when not coupled with analytical processes such as proteome and RNAome analysis. However, a typical benefit of FCS is the capacity for high throughput analysis of known protein–protein or protein–nucleotide interactions in solution. FCS coupled with these analytical strategies should be employed in the future to identify the interacting partners.

Many types of FP have been used as nuclear markers. These proteins are classified as two types: NLS peptides fused with oligomeric FP [10,11], and functional nuclear proteins (e.g., histone

H2B, ERK1, and importin β) fused with a monomeric FP [9,12]. In the former type, an increase in molecular weight resulting from oligomerization is important for inhibiting export from the nucleus. In the latter type, nuclear localization is likely to be mediated by retention of the protein in the nucleus. One benefit of using functional nuclear proteins as a tag is that it is easy to predict the localization of the fluorescent fusion protein (e.g., nucleoplasm, nuclear membrane, chromatin, and so on). Although both of these markers can be used for observation by fluorescence microscopy, one drawback is that they are difficult to use for artificial nuclear localization of a protein of interest for functional analysis. This is because the function of the tagged protein may be disturbed by oligomerization of the FP. Thus, GFP tagged with the appropriate NLS should result in less inhibition of function of the tagged partner protein. GFP-NLS^{SV40}, which shows clear localization in the nucleus *via* RNA binding but remains highly dynamic in living cells, can be used not only as a nuclear marker, but also as a tag that will not disturb the function of the fusion protein. Our NLS-tagging procedure is ideal for use in multiple applications, including competition assays to analyze nuclear import and artificial sequestration of proteins in the nucleus.

Conflict of interest

The authors declare that there are no conflicts of interest.

Acknowledgments

Transparency document

Transparency document related to this article can be found online at http://dx.doi.org/10.1016/j.bbrc.2015.05.084.

References

[1] F.M. Boisvert, S. van Koningsbruggen, J. Navascues, A.I. Lamond, The multifunctional nucleolus, Nat. Rev. Mol. Cell. Biol. 8 (2007) 574–585.

[2] I. Grummt, The nucleolus-guardian of cellular homeostasis and genome integrity, Chromosoma 122 (2013) 487–497.

[3] M. Hetman, M. Pietrzak, Emerging roles of the neuronal nucleolus, Trends Neurosci. 35 (2012) 305–314.

[4] A. Mor, M.A. White, B.M. Fontoura, Nuclear trafficking in health and disease, Curr. Opin. Cell Biol. 28 (2014) 28–35.

[5] I.W. Mattaj, L. Englmeier, Nucleocytoplasmic transport: the soluble phase, Annu. Rev. Biochem. 67 (1998) 265–306.

[6] A. Lange, R.E. Mills, C.J. Lange, M. Stewart, S.E. Devine, A.H. Corbett, Classical nuclear localization signals: definition, function, and interaction with importin alpha, J. Biol. Chem. 282 (2007) 5101–5105.

[7] D. Kalderon, B.L. Roberts, W.D. Richardson, A.E. Smith, A short amino acid sequence able to specify nuclear location, Cell 39 (1984) 499–509.

[8] B.J. Lee, A.E. Cansizoglu, K.E. Suel, T.H. Louis, Z. Zhang, Y.M. Chook, Rules for nuclear localization sequence recognition by karyopherin beta 2, Cell 126 (2006) 543–558.

[9] R. Ando, H. Mizuno, A. Miyawaki, Regulated fast nucleocytoplasmic shuttling observed by reversible protein highlighting, Science 306 (2004) 1370–1373.

[10] S. Chatterjee, M. Javier, U. Stochaj, In vivo analysis of nuclear protein traffic in mammalian cells, Exp. Cell Res. 236 (1997) 346–350.

[11] F. Rodrigues, M. van Hemert, H.Y. Steensma, M. Corte-Real, C. Leao, Red fluorescent protein (DsRed) as a reporter in Saccharomyces cerevisiae, J. Bacteriol. 183 (2001) 3791–3794.

[12] H. Kimura, P.R. Cook, Kinetics of core histones in living human cells: little exchange of H3 and H4 and some rapid exchange of H2B, J. Cell Biol. 153 (2001) 1341–1353.

[13] D.A. Zacharias, J.D. Violin, A.C. Newton, R.Y. Tsien, Partitioning of lipid-modified monomeric GFPs into membrane microdomains of live cells, Science 296 (2002) 913–916.

[14] V. Schreiber, F. Dantzer, J.C. Ame, G. de Murcia, Poly(ADP-ribose): novel functions for an old molecule, Nat. Rev. Mol. Cell. Biol. 7 (2006) 517–528.

[15] A.F. Fradkov, V.V. Verkhusha, D.B. Staroverov, M.E. Bulina, Y.G. Yanushevich, V.I. Martynov, S. Lukyanov, K.A. Lukyanov, Far-red fluorescent tag for protein labelling, Biochem. J. 368 (2002) 17–21.

[16] D. Axelrod, D.E. Koppel, J. Schlessinger, E. Elson, W.W. Webb, Mobility measurement by analysis of fluorescence photobleaching recovery kinetics, Biophys. J. 16 (1976) 1055–1069.

[17] D.M. Soumpasis, Theoretical analysis of fluorescence photobleaching recovery experiments, Biophys. J. 41 (1983) 95–97.

[18] A. Kitamura, N. Inada, H. Kubota, G. Matsumoto, M. Kinjo, R.I. Morimoto, K. Nagata, Dysregulation of the proteasome increases the toxicity of ALS-linked mutant SOD1, Genes Cells 19 (2014) 209–224.

[19] D. Morito, K. Nishikawa, J. Hoseki, A. Kitamura, Y. Kotani, K. Kiso, M. Kinjo, Y. Fujiyoshi, K. Nagata, Moyamoya disease-associated protein mysterin/RNF213 is a novel AAA+ ATPase, which dynamically changes its oligomeric state, Sci. Rep. 4 (2014) 4442.

[20] A. Kitamura, H. Kubota, C.G. Pack, G. Matsumoto, S. Hirayama, Y. Takahashi, H. Kimura, M. Kinjo, R.I. Morimoto, K. Nagata, Cytosolic chaperonin prevents polyglutamine toxicity with altering the aggregation state, Nat. Cell. Biol. 8 (2006) 1163–1170.

[21] R. Rigler, U. Mets, J. Widengren, P. Kask, Fluorescence correlation spectroscopy with high count rate and low-background - analysis of translational diffusion, Eur. Biophys. J. Biophys. 22 (1993) 169–175.

[22] C. Pack, K. Saito, M. Tamura, M. Kinjo, Microenvironment and effect of energy depletion in the nucleus analyzed by mobility of multiple oligomeric EGFPs, Biophys. J. 91 (2006) 3921–3936.

[23] J. Dresios, P. Panopoulos, D. Synetos, Eukaryotic ribosomal proteins lacking a eubacterial counterpart: important players in ribosomal function, Mol. Microbiol. 59 (2006) 1651–1663.